Journal of Power Sources 235 (2013) 297–302

Contents lists available at SciVerse ScienceDirect

Journal of Power Sources

journal homepage: www.elsevier.com/locate/jpowsour

Syntheses of size-varied nanorods TiO_2 and blending effects on efficiency for dye-sensitized solar cells

Ping-Lin Kuo [a,*], Tzung-Shiue Jan [a], Chun-Hou Liao [a], Chi-Chang Chen [a], Kun-Mu Lee [b]

[a] Department of Chemical Engineering, National Cheng Kung University, Tainan 70101, Taiwan, ROC
[b] Research Center for New Generation Photovoltaics, National Central University, Taoyuan 32001, Taiwan, ROC

ARTICLE INFO

Article history:
Received 5 July 2012
Received in revised form
10 September 2012
Accepted 12 September 2012
Available online 24 October 2012

Keywords:
Anatase titanium dioxide nanorod
Scattering
Blending
Dye-sensitized solar cells

ABSTRACT

A series of one-dimensional anatase nanorods TiO_2 with various lengths and aspect ratios are synthesized. The smallest rods TiO_2 (EOA) with a length of 20–40 nm and a width of about 5 nm possess extremely high surface area (151.5 $m^2\ g^{-1}$) compared to P25 (56.4 $m^2\ g^{-1}$) and the largest rods TiO_2 (TMA-L) with a length of 800 nm and a width of about 200 nm result in very low transmittance. The EOA show the lower R_w (charge transport resistance) and higher R_k (charge recombination resistance) than the P25. It indicates that the one-dimensional TiO_2 structure lowers the charge transport resistance by decreasing grain boundary and stretching grown structure with the specified directionality, and increases recombination reaction due to reducing the surface defects. A higher light-to-electricity conversion yield of 5.61% is achieved by applying the EOA as compared with P25 (5.08%). The TMA-L coat on the EOA film to form double-layer films enhances the efficiency from 5.61 to 5.84%, and the scattering layer of the blending of EOA and TMA-L coated on the EOA film raises the efficiency to 6.08%.

1. Introduction

The dye-sensitized solar cell (DSSC) is one of the low-cost, high-efficiency, and environmentally friendly solar cells [1]. A DSSC is composed of the high-surface-area TiO_2 film on a conducting glass substrate, high absorption efficiency sensitized-dye, counter electrode with platinum coating, and I^-/I_3^- redox electrolyte solution. The dynamics compete with DSSC for electron injection and dye regeneration, which occurs in the femtoseconds to nanoseconds time scale; however, the electron transport in the TiO_2 film and interfacial recombination on the TiO_2 surface due to I_3^- are in the milliseconds to seconds [2]. Therefore, the electron transport and the electron recombination are the key factors affecting the efficiency.

In order to increase electron transportation and to decrease interfacial recombination, one-dimensional nanostructured TiO_2 (nanotubes [3], nanorods [4] and nanowires [5–8]) were prepared. It was anticipated that they would have a single crystalline structure to facilitate incrementally electron transportation in the photoelectrode and less surface defects for reducing recombination on the TiO_2 surface. In addition to one-dimensional structured, DSSC has to emphasize the photoelectrode morphology. On the Arakawa group [9], they changed TiO_2 photoelectrodes with different structures, with layers of small particles, large particles, and mixture of small particles and large particles on the conducting glass. Small particles are essential to increase dye adsorption due to high surface area, while large particles are required to enhance red light absorption through light scattering. It is impossible to increase surface area and light scattering simultaneously, because they oppose each other. Therefore, a double-layer combining a transparent layer with high surface area and light-scattering layer with large particle size is the common method to reach high effect.

In this paper, a series of one-dimensional anatase nanorods TiO_2 were prepared by hydrothermal process using the synergist of different stabilizers and chelating agents to form TiO_2 nanorods with various lengths and aspect ratios. Those one-dimensional nanorods TiO_2 show the length in the range from 20 to 800 nm and the width in the range from 5 to 200 nm. The smallest rods TiO_2 (EOA) show transparent film with high surface area (151.5 $m^2\ g^{-1}$) and the largest rods TiO_2 (TMA-L) show 8% lower transmittance with high scattering. A higher light-to-electricity conversion yield of 5.61% was achieved by applying the high surface area EOA as compared with P25 (5.08%). Furthermore, the scattering layer of large rods (TMA-L, TMA-M, TMA-S) coated on the EOA film

* Corresponding author. Tel.: +886 6 275 7575; fax: +886 6 276 2331.
E-mail address: plkuo@mail.ncku.edu.tw (P.-L. Kuo).

0378-7753/$ – see front matter © 2012 Elsevier B.V. All rights reserved.
http://dx.doi.org/10.1016/j.jpowsour.2012.09.070

enhanced the efficiency from 5.61% to 5.84%, and the scattering layer of the blending of EOA and TMA-L coated on the EOA film increased the efficiency to 6.08%.

2. Experimental section

2.1. Preparation of TiO_2 particles and paste

The similar procedures for the preparation of one-dimensional nanorods TiO_2 were conducted according to the method reported by Sugimoto group [10,11]. First, titanium isopropoxide (TIPO) and ethanolamine were mixed at a molar ratio of TIPO/ethanolamine = 1/25 to form the compound Ti^{4+}, which is stable against hydrolysis at room temperature. This was followed by the addition of distilled water and NH_4OH solution to make the final solution of pH = 11. The final solution was placed in a Teflon-lined autoclave with a two-step hydrothermal process. The first step was carried out at 100 °C for 24 h to form a rigid gel of titanium hydroxide. The second step was aging at 150 °C for 72 h to finish the nucleation and grow of the one-dimensional TiO_2 designated as EOA. Besides, the scattering nanorods TiO_2 were produced by similar method. First, TIPO and triethanolamine were mixed at a molar ratio of 1/2. This was followed by the addition of distilled water, different quantities of acetyl acetone (ACA) that controls particle size. Then the solution use trimethylamine to control the pH = 11. The final solution was placed in a Teflon-lined autoclave and reacted at 100 °C for 24 h and 150 °C for 72 h. Those nanorods were designated according to their size from small to large as TMA-S, TMA-M, and TMA-L.

In this study, the TiO_2 paste was prepared by employing Graltzel's method [12]. First, the TiO_2 was dispersed in ethanol and then mixed with terpineol and ethyl cellulose. After removing the ethanol with a rotary-evaporator, the final paste was prepared. The terpineol-based paste is very stable at long-term and gives reproducible efficiency.

2.2. Preparation TiO_2 electrode

The fluorine-doped SnO_2 conducting glass was cleaned by surfactant, acetone and isopropanol, and applied the $TiCl_4$ post-treatment to make good mechanical contact between the TiO_2 layer and conducting glass. Then, the TiO_2 film was made by doctor blade and was heated at 450 °C for 15 min and at 500 °C for 15 min. The layer thickness was determined by Alpha-step IQ surface profilometer (Tencor Instruments, USA).

2.3. Nanorods and electrodes characterization

Characterization of the nanorods were made by X-ray diffraction (XRD) (Rigakue, RINT2000), transmission electron microscopy (TEM) (JEOL, JEM-1200EX), isotherm of nitrogen adsorption (Micromerit ASAP 2020). Characterization of the electrodes were made by field emission scanning electron microscope (FE-SEM) (JEOL, JSM-6700F) and ultraviolet–visible light spectrophotometer (Beckman, DU-800).

2.4. Fabrication of dye-sensitized solar cells and photoelectrochemical measurements

After sintering at 500 °C and cooling to 80 °C, the TiO_2 electrodes were dye-coated by immersing them into dye solutions at 60 °C for 16 h, which consisted of 0.5 mM N719 dye (Solaronix) in acetonitrile and tertiary butanol (in the volume ratio of 1:1). The dye-coated TiO_2 films and the Pt counter electrodes were assembled into sealed sandwich-type cells by heating with hot melt sealing foil (SX1170-25, 25 μm thickness, Solaronix) used as spacers between the electrodes. A drop of electrolyte solution (0.1 M LiI, 0.6 M DMPII, 0.05 M I_2, and 0.5 M TBP in methoxyacetonitrile) was introduced into the assembled cell. Photocurrent–voltage measurements were performed using an AM 1.5 solar simulator (100 mW cm^{-2}, SAN-EI, Model:XES-301S, Japan). The electrochemical impedance spectroscopy (EIS) measurements in this study were carried out applying bias of the open circuit voltage (V_{oc}) [13]. EIS measurement of cells was recorded in a frequency range from 0.05 Hz to 1 MHz with an ac amplitude of 10 mV. The incident photon to electron conversion efficiency (IPCE) measurement was performed using a similar data collection system, except recording was conducted under monochromatic light illumination at short-circuit conditions. The incident light was generated by a 300 W xenon lamp (Oriel) equipped with a monochromator (Oriel Cornerstone 260 1/4 m). The active area of the dye-coated TiO_2 film was 0.16 cm^2.

3. Results and discussion

The hydrothermal technique is an appropriate process for preparing nanostructured materials because particle size, morphology, and structures can be controlled by adjusting preparation stabilizers. A series of one-dimensional nanorods TiO_2 with various lengths and aspect ratios were prepared using different stabilizers through a two-step hydrothermal process, shown as the transmission electron micrographs (TEM) in Fig. 1. The EOA prepared under ethanolamine is the smallest size TiO_2 with a length of 20–50 nm and a width of about 5 nm (as shown in Fig. 1(a)). For Fig. 1(b)–(d), the prepared TiO_2 are arbitrarily controlled from small to large as TMA-S, TMA-M and TMA-L under triethanolamine, trimethylamine, and different quantities of acetyl acetone. This size-control mechanism can be explained in terms of the stabilizer capability of enhancing the nucleation rate in second aging. Reversely, that triethanolamine results in a bigger nanorods

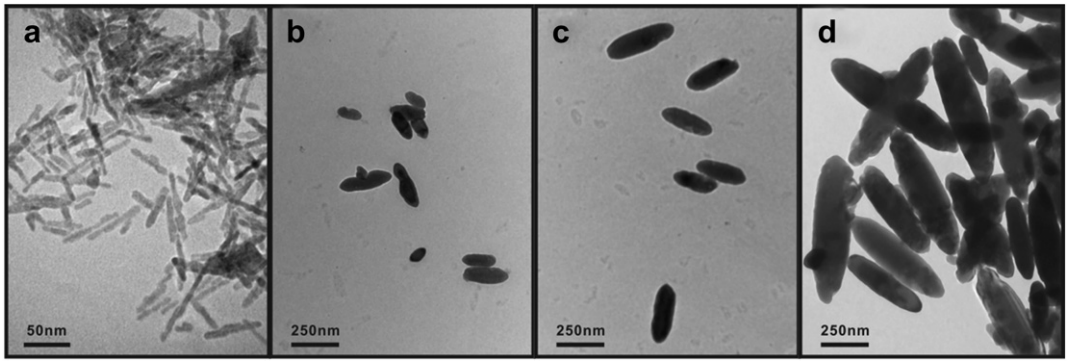

Fig. 1. TEM images for (a) EOA, (b) TMA-S, (c) TMA-M, (d) and TMA-L.

TiO_2, suggests its significant role working as a strong stabilizer to reduce the nucleation rate.

One-dimensional rod shape formation requires anisotropic crystal growth, which is realized usually when the surface free energies of the various crystallographic planes differ significantly. In general, addition of shape controller can adsorb on the highest-energy facets so that nucleation yield anisotropic crystal growth. According to Donnay–Harker rules, the surface free energy of the {001} faces is nearly 1.4 times larger than that of the {101} faces. Therefore, the ethanolamine and triethanolamine as shape controller can adsorb to the specific crystal faces parallel to the *c*-axis of the tetragonal system. In this study, ethanolamine and triethanolamine act not only as a stabilizer for TIPO to reduce the hydrolysis rate, but also as a shape controller to adsorb on the parallel *c*-axis surfaces of TiO_2 at high pH [10].

It is well known that the anatase form of TiO_2 is important for preparing efficient dye-sensitized solar cells [1]. The XRD patterns of the EOA, TMA-S, TMA-M and TMA-L are measured under the conditions of 40 kV and 30 mA and are shown in Fig. 2. The commercial powder P25 is also presented for comparison in Fig. 2. The P25 consists of two crystalline structures of anatase and rutile. For the EOA, TMA-S, TMA-M and TMA-L, the Fig. 2 shows that the peaks at 25.2°, 37.8° and 48° (TiO_2 anatase, JCPDS file 21-1272) correspond to the planes (101), (004), (200) [2], respectively, and evidence that the EOA, TMA-S, TMA-M and TMA-L are pure anatase.

The BET (Brunauer–Emmett–Teller) specific surface area of the commercial P25, via $TiCl_4$-fumed gas synthesis, is 56 $m^2\ g^{-1}$ and the pore distribution is from 2 to 86 nm (as shown in Fig. 3) with a BJH (Barrett–Joyner–Halenda) pore size of 17.7 nm. However, the BET surface area of the EOA (151.5 $m^2\ g^{-1}$) is higher than that of P25 (56.4 $m^2\ g^{-1}$). The BET results clearly indicate that there is an increase in surface area that can be attributed to the primary particle size. As compared with the primary particle size of P25, at 25–40 nm, the EOA has the smaller size of 5 nm short axes. The BJH pore size distribution of the EOA is relative narrow with an average pore diameter at ca. 3.9 nm.

In this study, the EOA paste is coated on FTO conducting glass to prepare photoelectrode which is subsequently sintered to form transparent mesoporous TiO_2 film. Compared to transparent mesoporous film, the TMA-L, TMA-M and TMA-S films are opaque even if the thickness is only 4 μm. Relative to these, the P25 film is semi-transparent (<5 μm) between EOA and TMA-S, becoming opaque gradually as the thickness increases.

Fig. 4 shows the transmittance spectra of the TiO_2 films made by P25, EOA, TMA-S, TMA-M, and TMA-L. The EOA film transmits 75%

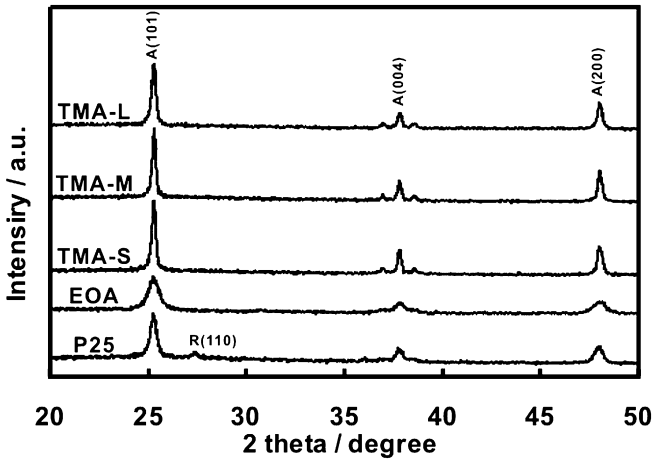

Fig. 2. XRD pattern for P25, EOA, TMA-S, TMA-M, and TMA-L.

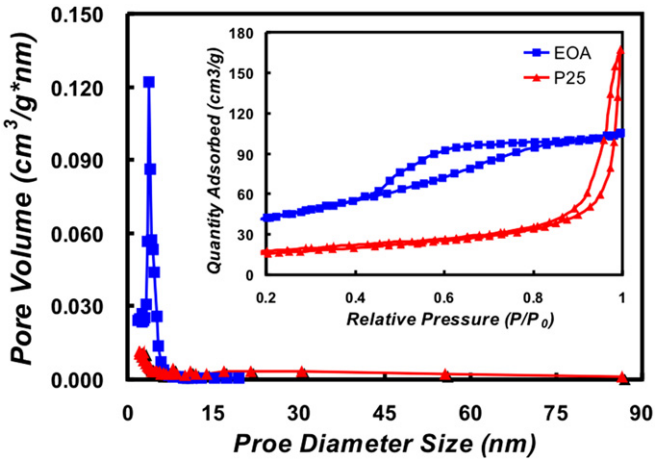

Fig. 3. Nitrogen adsorption isotherm pattern and the pore size distribution of the EOA and P25.

of incident light above 450 nm wavelength and exhibits excellent transparency. In comparison, the transmittance of P25 increases linearly from 375 to 600 nm wavelength, and the transmittance at 500 nm is half that of EOA. For the P25 film, the transmittance is lower than EOA even if the P25 primary particle size is only 25–40 nm. The reason is that the P25 presents rutile phase that is well known to be more efficient in scattering red light than anatase [14].

It has been reported that particles with the size over 100 nm can scatter visible light effectively [14–16]. In this study the TMA-L is able to diffuse visible light with transmittance less than 8% of incident light ranging from 300 to 800 nm. However, the TMA-M and TMA-S can only effectively scatter incident light below 550 nm so that the transmittance increases linearly from 550 to 800 nm wavelength, and thus TMA-M and TMA-S can not scatter the red region effectively.

The detailed morphology for the top surface of TiO_2 films is investigated by using field emission scanning electron microscopy (SEM). As shown in Fig. 5, all the films after calcination at 450 °C for 30 min are crack-free and the nanorods TiO_2 made via two-step hydrothermal process maintain the one-dimensional structure after calcinations. The result corroborates that the one-dimensional TiO_2 possess excellent thermal stability. As compared with the P25 film (Fig. 5(a)), the EOA film contains no aggregates and shows

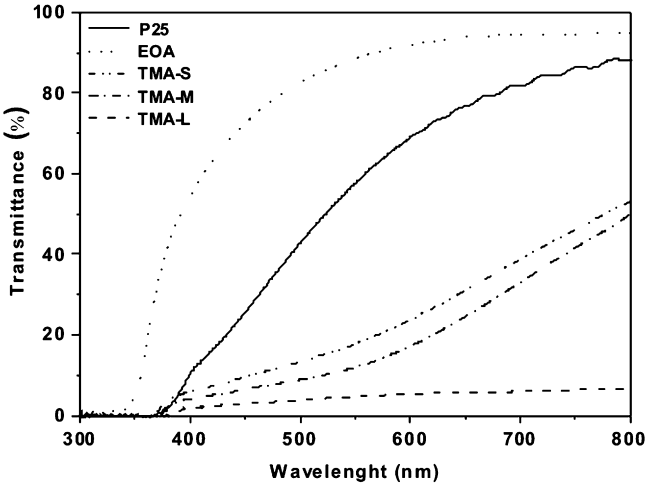

Fig. 4. Transmission spectra of the P25, EOA, TMA-S, TMA-M, and TMA-L films supported on FTO glass.

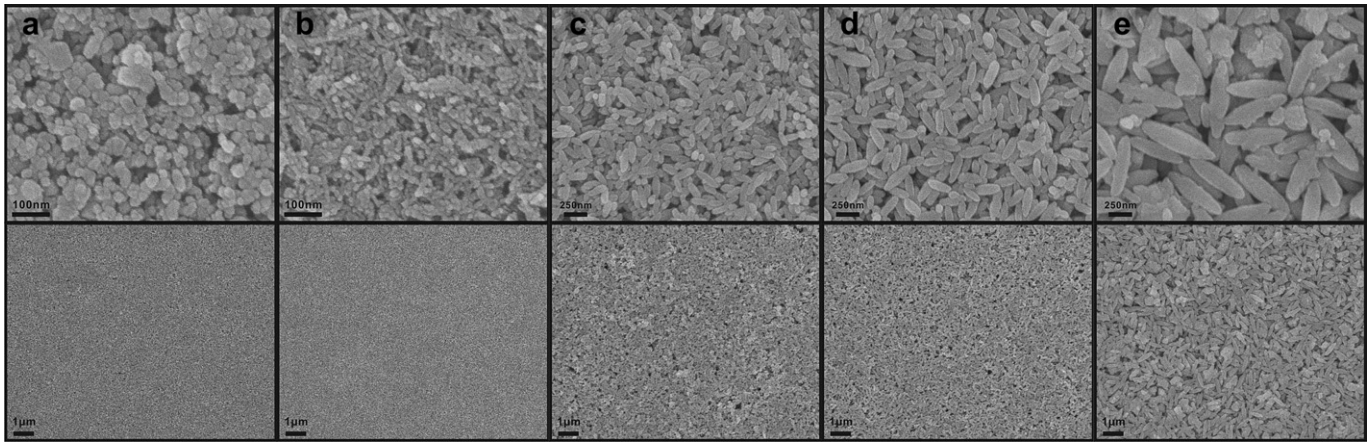

Fig. 5. Top view of SEM images for films made from (a) P25, (b) EOA, (c) TMA-S, (d) TMA-M, (e) and TMA-L.

Table 1
Photovoltaic performances of DSSC with different TiO_2 electrodes.

Photoelectrode	J_{SC} (mA cm^{-2})	V_{OC} (V)	*FF*	η (%)
EOA	11.32	0.73	0.68	5.61
EOA + TMA-S	11.67	0.73	0.65	5.52
EOA + TMA-M	11.59	0.73	0.68	5.76
EOA + TMA-L	11.60	0.74	0.68	5.84
P25	11.77	0.71	0.61	5.08
P25 + TMA-L	10.49	0.71	0.62	4.63

more compact structures (Fig. 5(a)). On the other hand, P25 shows the small aggregates and less compact structures with larger void spaces. The results correspond with the BJH analysis. Besides, it is well known that the surfaces roughness can influence the light scattering. For the TMA-S, TMA-M and TMA-L, the surfaces are rough and the level of roughness is correlated with the particles size (as shown in Fig. 5(c)–(e)). The results coincide with of UV spectrum, where the light scattering of TMA-L is most effective.

As mentioned above, the EOA has high surface area and transmittance, so it is a good material for the light-transmittance layer of DSSC. The TMA-L, TMA-M and TMA-S can be utilized as the scattering layer for DSSC capable for red light scattering. The performances of the single-layer film and double-layer film that are evaluated under 1 sun AM 1.5 simulated sunlight show in Table 1. The EOA exhibits higher V_{oc} and fill factor (*FF*) than the P25. The reason for the higher V_{oc} can be attributed to the maintained charge recombination by reducing surface defects (surface states, grain boundaries, self trapping etc.) due to the one-dimensional structure of EOA [17]. The *FF* is determined by the internal resistance of the cell. The resistance source comes from conducting glass, ion diffusion in the electrode-pore, electron conductibility in the electrode and counter electrode. The EOA film is characterized having the capability of higher electron transmission due to decreasing grain boundary and stretching grown structure with the specified directionality [17], so it displays low internal resistance that results in higher *FF*. An enhancement of light-to-electric conversion efficiency can be observed EOA (5.61%) is achieved as compared with P25 (5.08%).

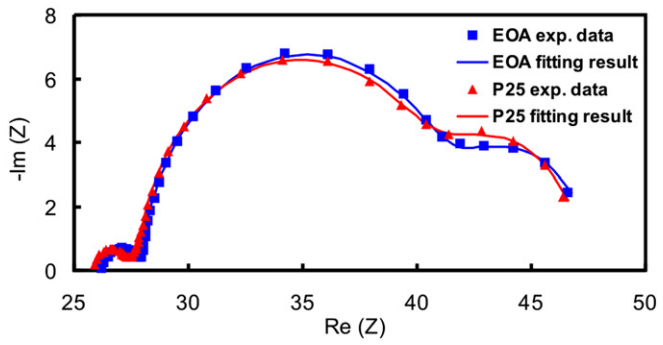

Fig. 6. Electrochemical impedance spectroscopy (EIS) for dye-sensitized solar cells with P25 and EOA, respectively.

In order to research the electron transport and charge recombination property in TiO_2 film electrodes, the electrochemical impedance spectroscopy (EIS) measurements are employed. The Fig. 6 shows the Nyquist plots of the EIS of EOA and P25. The Nyquist plots exhibit three semicircles including: (1) the high frequency semicircle which is assigned to the electron transfer at the Pt counter electrode [13,15,16]; (2) the central arc which is influenced by (i) charge transport resistance (R_w) ascribed to the accumulation/transport of the injected electrons in TiO_2 film and (ii) charge recombination resistance (R_k) occurred when the electron crosses either the TiO_2/redox electrolyte interface or the TiO_2/FTO interface [3,13,16,18–21]; (3) the low frequency semicircle which is attributed to diffusion resistance of I^-/I_3^- in the electrolyte [3,13,16,19–21].

From Fig. 6, a series of TiO_2 properties (R_w, R_k) for EOA and for the compared P25 were acquired by fitting the central arc in Nyquist plots of EIS as shown in Table 2. The R_w in the EOA was 0.55 Ω which is about 2/5 times for the P25, indicating that the one-dimensional TiO_2 structure lowers the charge transport resistance by decreasing grain boundary and stretching grown structure with the specified directionality. The charge transport resistance, a kind of the internal resistance, was to increase *FF* when reduced by one-dimensional structure. The result coincided with the DSSC performances (Table 1), where the EOA display higher *FF* than the P25. Moreover, the R_k value was 12.4 Ω for the EOA and 11.8 Ω for the P25, showing that the recombination reaction was prevented by the EOA owing to with reducing the surface defects. A small difference in V_{oc} observed in Table 1 agreed with R_k value for EOA and P25.

Table 2
Properties of DSSC determined by electrochemical impedance spectroscopy (EIS) measurements.

	D_{eff} (cm^2 s^{-1})	K_{eff} (s^{-1})	τ_{eff} (s)	R_k (Ω)	R_w (Ω)	L (μm)
EOA	4.87×10^{-4}	15.0	0.066	12.4	0.55	12
P25	1.74×10^{-4}	8.01	0.125	11.8	1.39	16

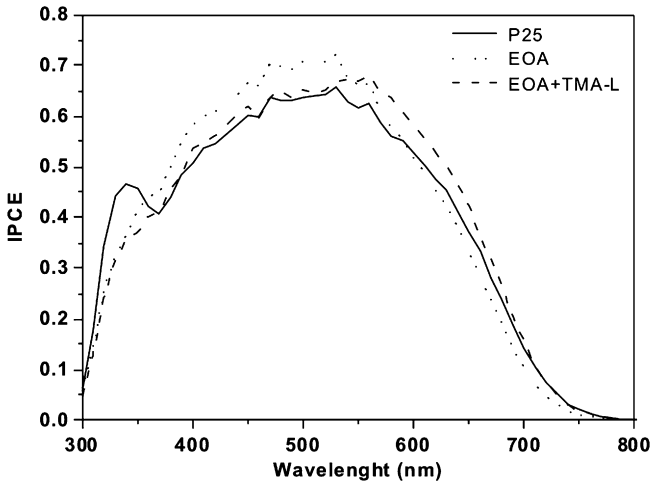

Fig. 7. Incident photon to current conversion efficiency (IPCE) curves of DSSCs with TiO_2 electrodes prepared from P25, EOA, and EOA + TMA-L, respectively.

For the EOA, the J_{sc} is slightly lower than P25 despite that EOA shows higher surface area. The EOA film is to transmittance to employ the red light range sufficiently. In order to increase red light absorption, the study uses double-layer method by adding the scattering layer on EOA film to increase the incident light scattering. For the EOA + TMA-L, it presents the best light-to-electric energy conversion efficiency, because the TMA-L reveal the best scatting effect, as shown in Fig. 4. Further analysis of the J_{sc} is performed by incident photon-to-current efficiency (IPCE), which is defined as the ratio of collected electrons to incident photons. In Fig. 7, the IPCE of EOA is highest in the range of 300–550 nm, but it becomes worst in red light range. However, when the EOA film is coated with TMA-L layers, the IPCE is increased in the range of 550–800 nm, resulting in the best light-to-electric energy conversion efficiency.

In order to increase the efficiency of scattering layer further, EOA is used to blend TMA-L to increase surface area of scattering layer to adsorb more dye. Surface analyses of the EL13, EL11 and EL31 are carried out by SEM (as shown in Fig. 8(a)–(c)). From the surfaces of the films, they can be observed that the particles of EOA and TMA-L

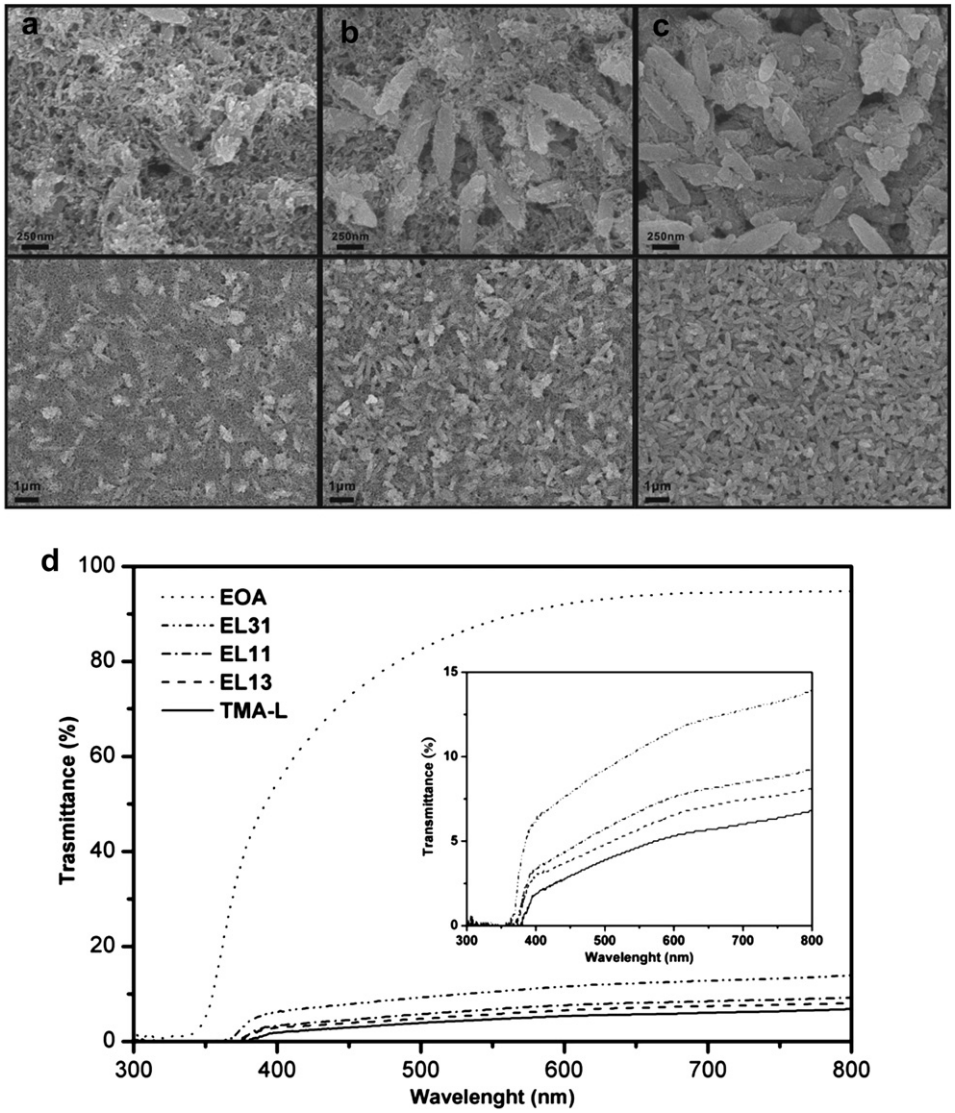

Fig. 8. Top view of SEM images for films made from (a) EL13, (b) EL11, (c) and EL31. (d) Transmission spectra of the P25, EOA, EL13, EL11, EL31, and TMA-L films supported on conducting glass.

Table 3
Photovoltaic performances of DSSC with different scattering layer from EL31, EL11, EL13 and TMA-L.

Photoelectrode	J_{SC} (mA cm^{-2})	V_{OC} (V)	*FF*	η (%)
EOA + EL31	11.14	0.72	0.67	5.43
EOA + EL11	12.69	0.73	0.66	6.08
EOA + EL13	11.87	0.74	0.66	5.86
EOA + TMA-L	11.60	0.74	0.68	5.84

are homogeneously dispersed and the surfaces are crack-free over the large area. As the ratio of the TMA-L is increased, the surfaces showed higher roughness with large void spaces of several hundred nm in size due to the TMA-L and less compact structure with less surface area. As shown in Fig. 8(d), the transmittances of EL13, EL11 and EL31 were lower than that of EOA and gradually increased with increasing EOA content. As compared with TMA-L, the transmittances of the EL13 and EL11 are slightly increased with 1.2% and 2.2%, respectively, in the range from 400 to 800 nm wavelength, where the blending of 50 wt % EOA to TMA-L (EL11) did not change the scattering effect dramatically. However, the EL31 layer transmitted 12.8% of incident light in 700 nm wavelength, more than twice that of TMA-L, and this maybe influence scattering red light effect.

The performances of the double-layer-films with scattering layer for EL31, EL11, EL13 and TMA-L that are measured under 1 sun (AM 1.5) simulated sunlight show in Table 3. The V_{OC} and *FF* indicated almost the same values at each case. The EL11 carried out the largest J_{SC}, which is due to the high surface area and light scattering effect. As compared with EL11, the EL13 had low surface area and the EL31 had low light scattering effect. The highest efficiency of 6.08% was obtained when DSSC with EL11 TiO2 electrode, while the η of that with EL31, EL13 and TMA-L were lower, as 5.43%, 5.86% and 5.84%, respectively. For the sake of investigating the definite effect on light absorption efficiency due to the EL11 and TMA-L, we used the IPCE, which is defined as the ratio of collected electrons to incident photons. Compared with TMA-L, the significantly improved IPCEs below 550 nm of EL11 are persuasive evidence for the efficient increasing of surface area (Fig. 9). Contrary to the remarkable improvement of IPCEs below 550 nm, EL11 gave lower IPCEs above 550 nm than TMA-L. As a consequence, the overall yield of EL11 is slightly higher than that of TMA-L. The overall yield is, therefore, increased from 5.84 to 6.08% by adjusting the scattering layer from TMA-L to EL11.

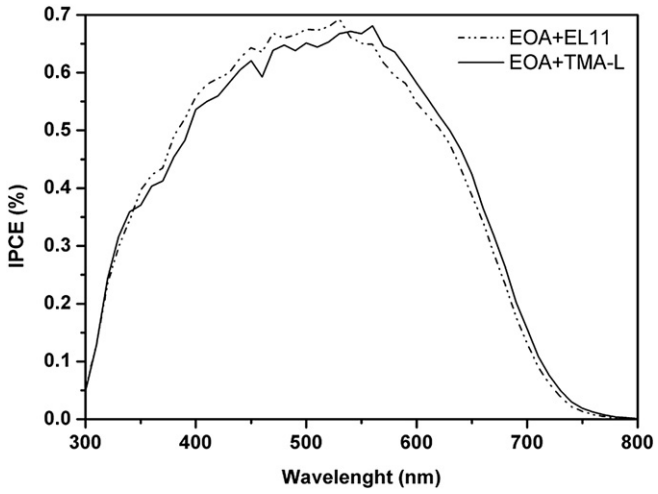

Fig. 9. Incident photon to current conversion efficiency curves of DSSC with TiO_2 electrodes prepared from EOA + EL11 and EOA + TMA-L, respectively.

4. Conclusions

In this study, a series of one-dimensional anatase nanorods TiO_2 were prepared using different stabilizers and chelations through a hydrothermal process. The EOA with a length of 20–40 nm and a width of about 5 nm possess high surface area (151.5 m^2 g^{-1}) compared to that of P25 (56.4 m^2 g^{-1}). The EOA shown the lower R_w and higher R_k than the P25, indicating that the one-dimensional TiO_2 structure not only lowers the charge transport resistance through decreasing grain boundary and stretching grown structure with the specified directionality, but also increases recombination reaction through reducing the surface defects. A higher light-to-electricity conversion yield of 5.61% was achieved by applying the high surface area EOA as compared with P25 (5.08%). The largest rods TiO_2 (TMA-L) with a length of 800 nm and a width of about 200 nm result in very low transmittance, less than 8% of incident light ranging from 300 nm to 800 nm. The TMA-L was added on the EOA film to form double-layer films, which enhanced the efficiency from 5.61 to 5.84%. Furthermore, the scattering layer of the blending of EOA and TMA-L was on the EOA film, which increased the efficiency to 6.08%.

Acknowledgments

The authors would like to thank the National Science Council, Taipei, ROC for their generous financial support of this research.

Appendix A. Supplementary data

Supplementary data related to this article can be found at http://dx.doi.org/10.1016/j.jpowsour.2012.09.070.

References

[1] N.G. Park, J. van de Lagemaat, A.J. Frank, The Journal of Physical Chemistry B 104 (2000) 8989–8994.
[2] M. Adachi, Y. Murata, J. Takao, J.T. Jiu, M. Sakamoto, F.M. Wang, Journal of the American Chemical Society 126 (2004) 14943–14949.
[3] H. Xu, X. Tao, D.-T. Wang, Y.-Z. Zheng, J.-F. Chen, Electrochimica Acta 55 (2010) 2280–2285.
[4] J. Jiu, S. Isoda, F. Wang, M. Adachi, The Journal of Physical Chemistry B 110 (2006) 2087–2092.
[5] Y.S. Beppu Takayuki, Hayase Shuzi, The Japan Society of Applied Physics 46 (2007) 4307–4311.
[6] B. Tan, Y. Wu, The Journal of Physical Chemistry B 110 (2006) 15932–15938.
[7] K. Asagoe, S. Ngamsinlapasathian, Y. Suzuki, S. Yoshikawa, Central European Journal of Chemistry 5 (2007) 605–619.
[8] J.-K. Oh, J.-K. Lee, H.-S. Kim, S.-B. Han, K.-W. Park, Chemistry of Materials 22 (2009) 1114–1118.
[9] Z.-S. Wang, H. Kawauchi, T. Kashima, H. Arakawa, Coordination Chemistry Reviews 248 (2004) 1381–1389.
[10] T. Sugimoto, X. Zhou, A. Muramatsu, Journal of Colloid and Interface Science 259 (2003) 43–52.
[11] T. Sugimoto, X. Zhou, A. Muramatsu, Journal of Colloid and Interface Science 259 (2003) 53–61.
[12] S. Ito, P. Chen, P. Comte, M.K. Nazeeruddin, P. Liska, P. Péchy, M. Grätzel, Progress in Photovoltaics: Research and Applications 15 (2007) 603–612.
[13] M. Adachi, M. Sakamoto, J. Jiu, Y. Ogata, S. Isoda, The Journal of Physical Chemistry B 110 (2006) 13872–13880.
[14] G. Rothenberger, P. Comte, M. Grätzel, Solar Energy Materials and Solar Cells 58 (1999) 321–336.
[15] Y. Tachibana, K. Hara, K. Sayama, H. Arakawa, Chemistry of Materials 14 (2002) 2527–2535.
[16] S. Ito, S. Yoshida, T. Watanabe, Chemistry Letters 29 (2000) 70–71.
[17] S.H. Kang, S.H. Choi, M.S. Kang, J.Y. Kim, H.S. Kim, T. Hyeon, Y.E. Sung, Advanced Materials 20 (2008) 54–58.
[18] A. Hauch, A. Georg, Electrochimica Acta 46 (2001) 3457–3466.
[19] L. Han, N. Koide, Y. Chiba, T. Mitate, Applied Physics Letters 84 (2004) 2433–2435.
[20] T. Hoshikawa, M. Yamada, R. Kikuchi, K. Eguchi, Journal of the Electrochemical Society 152 (2005) E68–E73.
[21] T. Hoshikawa, T. Ikebe, R. Kikuchi, K. Eguchi, Electrochimica Acta 51 (2006) 5286–5294.